VOLUME 32 NUMBER 1 January 2026
pISSN 2287-2728
eISSN 2387-285X

CLINICAL and MOLECULAR HEPATOLOGY

The forum for latest knowledge of hepatobiliary diseases

Bacteroides eggerthii for MASLD

Infiltrative HCC as an immunotherapy-resistant subtype
SGLT2 inhibitors and liver fibrosis progression
Aspirin and HCC risk in MASLD
Hypothyroidism and liver-related events

KASL

pISSN 2287-2728
eISSN 2287-285X

CLINICAL and MOLECULAR HEPATOLOGY

https://doi.org/10.3350/cmh.2025.0475
Clinical and Molecular Hepatology 2026;32:239-257

Original Article

Bacteroides eggerthii ameliorates metabolic dysfunction-associated steatotic liver disease through host–microbe signaling and highlights 2-hydroxyisocaproate as a potential effector

Jiyi Choi[1,2,*], Moon Gyeong Yoon[1,*], Se Ha Jang[1,2], Geum Ok Baek[1], Hyun Sun Jung[1], Na-Rae Lee[3], Choong Hwan Lee[3], Ji Eun Han[1], Jae Youn Cheong[1], Jung Woo Eun[1], and Soon Sun Kim[1]

[1]Department of Gastroenterology, Ajou University School of Medicine; [2]Department of Biomedical Sciences, Ajou University Graduate School of Medicine, Suwon; [3]MetaMass Corp., Seoul, Korea

Graphical Abstract

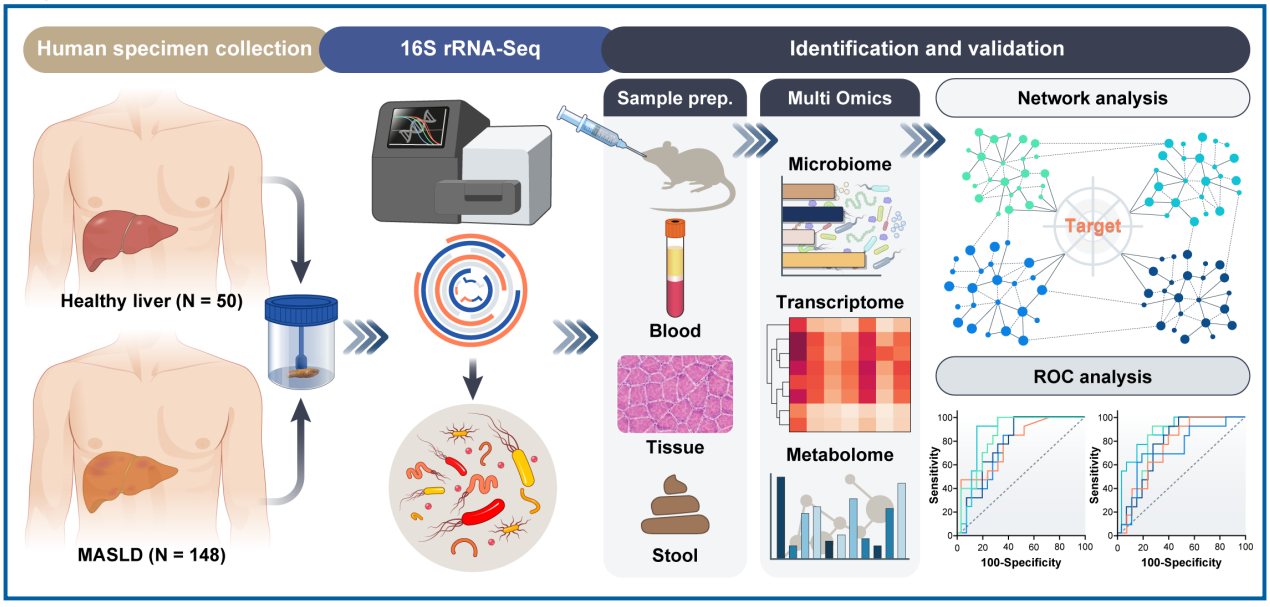

Study Highlights

- *Bacteroides eggerthii* was identified as a significantly depleted strain in both MASLD and obese patients through 16S rRNA-based microbiome analysis.
- *B. eggerthii* supplementation ameliorated MASLD phenotypes in a WD-induced mouse model, restoring gut microbial composition and host transcriptional pathways including FXR–FGF15–CYP8B1.
- Untargeted metabolomics revealed HICA as a *B. eggerthii*–derived metabolite consistently elevated in both feces and bacterial culture supernatant.
- *In vitro* validation confirmed that HICA reduced fatty acid–induced lipid accumulation in hepatocyte models, supporting its anti-steatotic effect as a microbiome-derived metabolite.

Background/Aims: Gut microbiome plays a pivotal role in metabolic dysfunction-associated steatotic liver disease (MASLD) pathogenesis, yet, associated functional mechanisms and host responses of specific microbial species remain insufficiently characterized. This study investigated the *Bacteroides eggerthii* therapeutic effects on MASLD by integrating multi-omics analysis and experimental validation in a Western diet (WD)-induced mouse model.

Methods: Candidate strains were identified using 16S rRNA gene sequencing of fecal samples from individuals with and without MASLD or obesity. *B. eggerthii*, a species significantly depleted in both groups, was selected for functional evaluation. Male C57BL/6J mice were fed a WD or WD supplemented with *B. eggerthii* (WD+B) for 12 weeks. Liver histology, serum biochemistry, fecal microbiome and metabolome profiling, and hepatic and intestinal transcriptomic analyses were performed. Anti-steatotic effects of *B. eggerthii*–derived metabolites were validated *in vitro*.

Results: *Bacteroides eggerthii* supplementation significantly improved liver weight, inflammation, fibrosis, and steatosis in WD+B group compared to WD alone. PICRUSt-based LEfSe analysis revealed choloylglycine hydrolase activity enrichment in gut microbiota, and strain-specific qPCR confirmed colonization in mouse colon. Integrated transcriptomic analyses revealed lipid and bile acid signaling pathway restoration, including CD36, FXR, and FGF15. Untargeted metabolomics identified elevated 2-hydroxyisocaproic acid (HICA) as a strain-derived metabolite in feces and *B. eggerthii* culture supernatants. *In vitro*, HICA significantly reduced lipid accumulation in free fatty acid-induced steatosis models.

Conclusions: *Bacteroides eggerthii* ameliorates MASLD via gut-liver axis modulation, including bile acid metabolism and hepatic lipid signaling. These underscore its therapeutic potential and highlight HICA as a novel microbiome-derived metabolite with anti-steatotic activity. **(Clin Mol Hepatol 2026;32:239-257)**

Keywords: Metabolic dysfunction-associated steatotic liver disease; Gut microbiome; Obesity; *Bacteroides eggerthii*; 2-Hydroxyisocaproic acid

INTRODUCTION

Metabolic dysfunction-associated steatotic liver disease (MASLD), a chronic liver disease closely associated with metabolic syndrome and obesity, is characterized by the accumulation of fat within hepatocytes.[1] MASLD can progress to more severe forms such as metabolic dysfunction-associated steatohepatitis, fibrosis, and cirrhosis.[2] With the global rise in obesity and type 2 diabetes, MASLD has been reported to occur in approximately 25–30% of the

Corresponding author : Jung Woo Eun
Department of Gastroenterology, Ajou University School of Medicine, Worldcup-ro 164, Yeongtong-Gu, Suwon 16499, Korea
Tel: +82-31-219-4681, Fax: +82-31-219-4680, E-mail: jetaimebin@aumc.ac.kr
https://orcid.org/0000-0002-2461-6702

Soon Sun Kim
Department of Gastroenterology, Ajou University School of Medicine, Worldcup-ro 164, Yeongtong-Gu, Suwon 16499, Korea
Tel: +82-31-219-7822, Fax: +82-31-219-7820, E-mail: soonsunkim@aumc.ac.kr
https://orcid.org/0000-0002-6862-1896

*JC and MGY contributed equally to this work.

Editor: Hyun Ju You, Seoul National University, Korea

Received : May 4, 2025 / **Revised :** Oct. 20, 2025 / **Accepted :** Oct. 21, 2025

Abbreviations:

ALT, alanine aminotransferase; AST, aspartate aminotransferase; BMI, body mass index; CAP score, Controlled Attenuation Parameter score; GSEA, gene set enrichment analysis; H&E, hematoxylin and eosin; IHC, immunohistochemistry; KHIDI, Korea health industry development institute; kPa, Kilopascal; LDA, linear discriminant analysis; LDL, low-density lipoprotein; LEfSe, linear discriminant analysis effect size; MASLD, metabolic dysfunction-associated steatotic liver disease; M&T, Masson's trichrome; ND, normal diet; NAS, nonalcoholic fatty liver disease activity score; PCoA, principal coordinate analysis; qRT-PCR, quantitative real-time polymerase chain reaction; ROC, receiver operating characteristic; WD, Western diet

population worldwide, thereby becoming an important research focus.[3] Currently, effective microbiome-based treatments for MASLD in humans remain unclear, with lifestyle modifications, including diet and exercise, being the primary therapeutic options.[4,5]

Recently, the gut microbial community has emerged as a key factor in liver disease along the gut–liver axis, influencing disease onset, progression, and therapeutic response.[6] Obesity is accompanied by general dysbiosis—most notably a higher Firmicutes/Bacteroidetes (F/B) ratio and increased energy-harvesting capacity. In contrast, MASLD exhibits disease-specific microbial signatures that implicate bile-acid metabolism, choline utilization, and inflammatory pathways, as summarized in recent reviews.[7-9] As a Western diet (WD) induces both obesity and hepatic steatosis, disentangling obesity-related shifts from MASLD-specific alterations is essential. This rationale motivated us to compare healthy controls with two MASLD subgroups (non-obese MASLD and obese MASLD) and to use a WD mouse model to probe causality *in vivo*. In this framework, distinct alterations in gut communities have been linked to MASLD progression, wherein imbalances can exacerbate hepatic inflammation, lipid accumulation, and metabolic dysregulation.[10] Harnessing the microbiome for diagnosis, prevention, and therapy therefore remains an attractive avenue for liver diseases.[11]

Among taxa differing between MASLD/obesity and healthy controls, we prioritized *Bacteroides eggerthii* based on its consistent depletion in patients, commercial availability for experimental validation, and literature suggesting immunometabolic relevance (e.g., weak TLR4 activation by lipooligosaccharides).[12,13] Reports linking *Bacteroides* spp. to bile acid deconjugation and short-chain fatty acids production further support a plausible metabolic interface with host pathways. These considerations informed our selection of *B. eggerthii* for *in vivo* testing. Here, we first delineated obesity-related versus MASLD-specific microbial alterations in humans by comparing healthy controls, non-obese MASLD, and obese MASLD. We then prioritized *B. eggerthii* and evaluated its effects in a WD-induced mouse model using an integrative multi-omics framework (16S profiling, fecal metabolomics, and hepatic/intestinal transcriptomics).

MATERIALS AND METHODS

Patients

Fecal samples and clinical data from healthy individuals (n=50) and patients with MASLD (n=148) were obtained from the Ajou University Hospital Biobank in Suwon, Korea. Patients with MASLD were recruited from the hepatology outpatient clinic of Ajou University Hospital based on clinical assessment and imaging criteria consistent with MASLD. The diagnosis of MASLD was based on the presence of hepatic steatosis confirmed by imaging or histology, at least one cardiometabolic risk factor, and no history of significant alcohol consumption (≥30 g/day for male, ≥20 g/day for female).[1] Healthy controls were recruited through institutional advertisements targeting individuals who visited the hospital or health screening center. Inclusion criteria for healthy controls included a body mass index (BMI) <25 kg/m^2, no history of excessive alcohol consumption, and no evidence of hepatic steatosis or other chronic liver diseases, including viral hepatitis. All controls underwent abdominal ultrasonography to exclude steatotic liver disease, and serologic tests were performed to exclude hepatitis B and C virus infection. FibroScan® (Echosens, Paris, France) was provided free of charge to all healthy participants. Fecal samples were obtained at various times during the day using a standardized plastic collection kit and stored at −80°C until analysis. All clinical information and biospecimens were anonymized and donated to the Ajou University Hospital Biobank in accordance with institutional ethical guidelines.

Among the 148 patients with MASLD, those with a body mass index (BMI) of ≥25 kg/m^2 were classified into the obese MASLD subgroup (n=110), whereas those with BMI <25 kg/m^2 were classified as the non-obese MASLD subgroup (n=38). Baseline characteristics of healthy controls, non-obese MASLD, and obese MASLD are presented in Supplementary Table 1.

This study was approved by the Institutional Review Board of Ajou University Hospital, Suwon, Korea (AJOUIRB-EX-2024-020 and AJOUIRB-SUR-2019-096). The use of anonymized fecal samples and clinical information was approved by the Ajou University Hospital Biobank, and the need for informed consent was waived.

Further experimental details are available in the online

supplementary materials and methods section.

Patient and public involvement

Patients or the public were not directly involved in the design, conduct, reporting, or dissemination plans of this research. However, the study utilized human-derived fecal samples obtained from the Ajou University Hospital Biobank, and all procedures were conducted following ethical guidelines. The research question and outcome measures were informed by current clinical priorities in the field of MASLD and gut microbiome research. The findings of this study will be shared with relevant clinical and scientific communities to inform future patient-centered research and therapeutic strategies.

RESULTS

Microbiome community composition and clinical features in the healthy, MASLD, and obesity groups

We analyzed the gut microbiome composition in the healthy, MASLD, and obesity groups using 16S rRNA sequencing (Fig. 1A). At the phylum level, the MASLD and obesity groups exhibited increased proportion of Firmicutes and reduced proportion of Bacteroidetes compared with the healthy group. This shift resulted in a higher F/B ratio in both MASLD and obesity groups, suggesting a gut microbiome imbalance associated with disease progression. At the class level, the MASLD and obesity groups demonstrated a higher abundance of Negativicutes and Bacilli and a decreased abundance of Bacteroidia than the healthy group. At the order and family levels, Selenomonadales, Lactobacillales, Veillonellaceae, and Lactobacillaceae were enriched, while Bacteroidales and Bacteroidaceae were reduced in MASLD and obesity groups.

To assess microbial diversity, we evaluated alpha diversity using OTUs and the ACE, Chao, and Shannon indices (Fig. 1B). Both the MASLD and obesity group exhibited significantly reduced alpha diversity compared with the healthy group, suggesting a loss of microbial richness and evenness. For beta diversity, PCoA based on Bray–Curtis dissimilarity did not show significant clustering differences among the three groups (R^2=0.0145, F=1.43, *P*=0.196) (Fig. 1C), indicating that while overall diversity was affected, the structural composition of the microbial communities remained relatively similar.

To systematically evaluate the association between gut microbial composition and clinical characteristics, we performed multivariable association analysis using MaAsLin2 across the entire cohort (n=198). Age, sex, BMI, and recent antibiotic use were included as covariates to adjust for their known influence on microbiome composition and clinical parameters. The abundance of Bacteroidetes was negatively associated with triglyceride levels, hepatic steatosis, and Controlled Attenuation Parameter (CAP) score, whereas Actinobacteria showed positive associations with triglyceride, CAP score, and liver stiffness (Fibro_Kilopascal [kPa]). In addition, Fusobacteria abundance was positively associated with dyslipidemia, triglyceride, and HbA1c. Proteobacteria levels correlated positively with MASLD, but negatively with hypertension (Fig. 1D). Further analysis revealed that Pseudoflavonifractor abundance negatively correlated with BMI, showing the highest predictive area under the curve (AUC) value (0.68). Lachnospira abundance positively correlated with liver steatosis (AUC 0.67). Proteobacteria levels increased with advancing fibrosis stages (AUC 0.73), while Erysipelotrichaceae abundance declined in advanced fibrosis stages, demonstrating the highest predictive AUC value (0.80) (Fig. 1E).

LEfSe was performed to identify differential abundant taxa among the groups. *Blautia wexlerae*, *Ruminococcus gnavus*, and *Blautia hansenii* group were consistently enriched in both MASLD and obesity compared with the healthy group (Fig. 1F). In total, 16 microbial taxa exhibited significant differences of the MASLD and obesity groups compared to the healthy group. Notably, *Alistipes putredinis*, *Alistipes shahii*, *B. eggerthii*, and *B. uniformis* decreased, whereas *Blautia hansenii*, *B. wexlerae*, and *R. gnavus* increased in the MASLD and obesity groups (Fig. 1G).

To investigate potential microbial candidates with ameliorative effects on MASLD and obesity, we focused on the taxa that were consistently decreased in disease conditions. Three taxa, *B. uniformis*, *A. putredinis*, and *B. eggerthii* were prioritized for further evaluation according to linear discriminant analysis (LDA) effect size. B. uniformis exhibited the highest LDA effect size (LDA=4.06 for

https://doi.org/10.3350/cmh.2025.0475

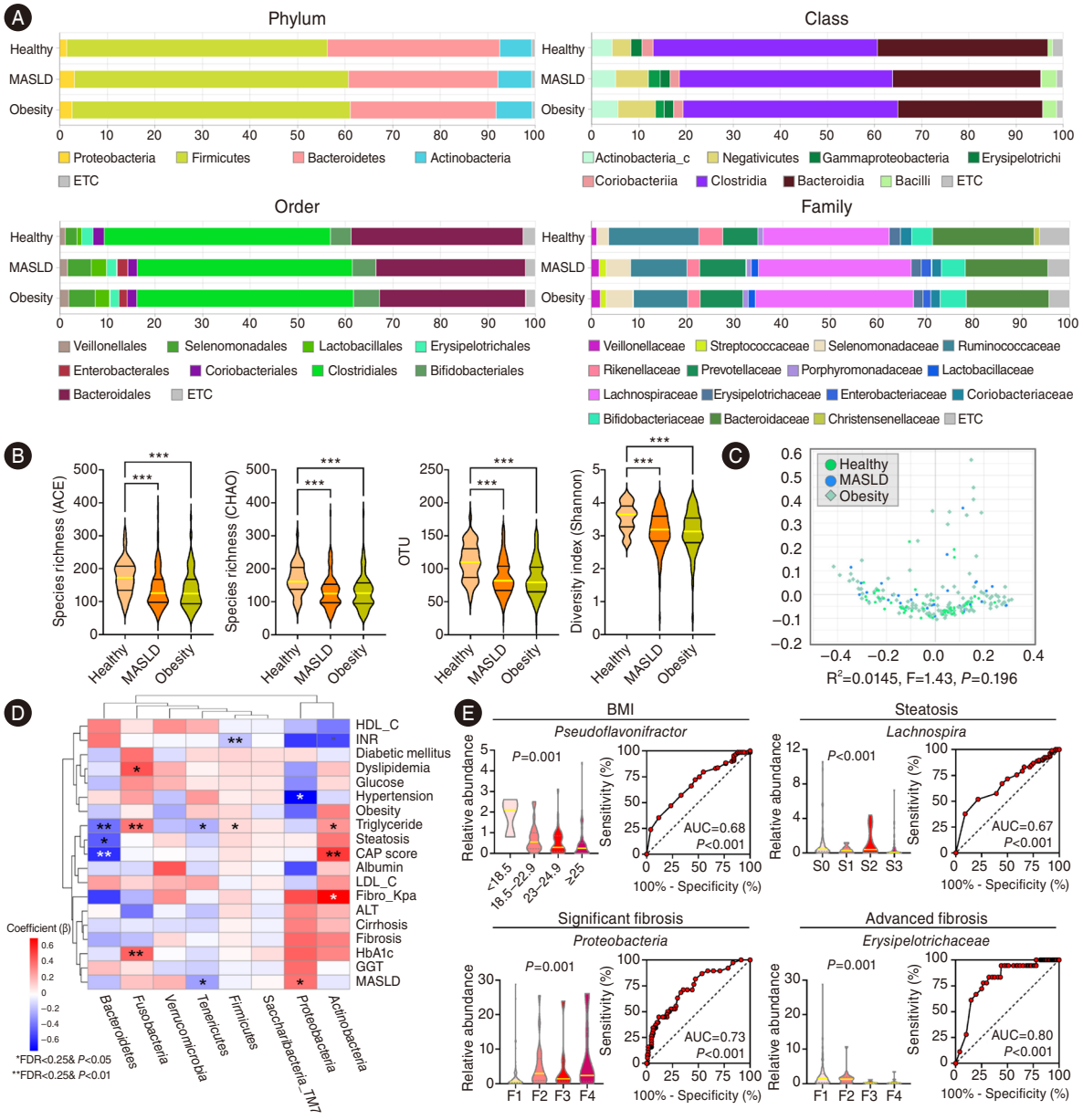

Figure 1. Gut microbiome composition and diversity in the healthy control (Healthy), metabolic dysfunction-associated steatotic liver disease (MASLD, combined cohort), and the obese MASLD subgroup ("Obesity") (MASLD=non-obese+obese MASLD; Obesity=obese MASLD only, BMI≥25 kg/m^2). (A) Relative gut microbiota abundance at the phylum, class, order, and family levels across Healthy, MASLD (combined), and Obesity (obese MASLD). (B) Alpha diversity analysis, including ACE, Chao1, OTU count, and Shannon indices, showing a significant reduction in microbial diversity in MASLD and obesity groups compared to Healthy. (C) Principal coordinates analysis of fecal microbiota composition based on Bray–Curtis dissimilarity among Healthy (green circles), MASLD (blue circles), and Obesity (cyan diamonds) subjects. Dashed ellipses represent 95% confidence intervals. PERMANOVA analysis did not detect significant differences in microbial beta diversity across groups (R^2=0.0145, F=1.43, *P*=0.196). (D) Clustered heatmap of MaAsLin2 coefficients (β) between phylum-level microbiome and clinical variables. Red indicates positive associations, blue negative. Stars indicate statistical significance: *P*<0.05 (*), *P*<0.01 (**), with FDR<0.25. (E) For each indicated taxon, the left violin plot shows its relative abundance across the entire cohort (all participants). The right panel shows receiver operating characteristic curves classifying healthy controls (HC) versus the MASLD combined cohort (non-obese+obese MASLD). Pseudoflavonifractor, Lachnospira, Proteobacteria, and Erysipelotrichaceae were identified as key taxa. (F) Linear discriminant analysis effect size analysis showing differentially enriched bacterial taxa among healthy, MASLD (combined), and Obesity (obese MASLD). Taxa with Linear Discriminant Analysis (LDA) score >2.0 and *P*<0.05 are shown. Bar colors indicate the enriched group: light orange (healthy), dark orange (MASLD), olive green (obesity). (G) Differentially enriched microbial taxa in the MASLD (combined) and Obesity (obese MASLD) compared to the ND group, highlight the potential microbial biomarkers for disease progression. Statistically significant differences were determined using one-way analysis of variance (ANOVA) with Tukey's *post-hoc* test; ***P<0.001.

 https://doi.org/10.3350/cmh.2025.0475

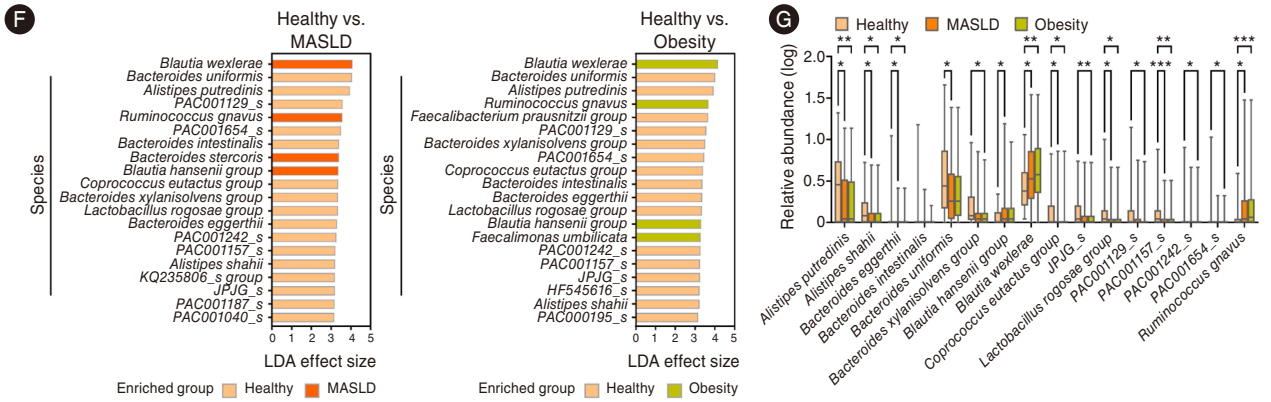

Figure 1. Continued.

MASLD; 4.00 for obesity), followed by *A. putredinis* (LDA=3.94 and 3.93) and *B. eggerthii* (LDA=3.28 and 3.34). *B. uniformis* has already been extensively characterized as a probiotic with beneficial effects in high-fat diet–induced metabolic dysfunction (Supplementary Table 2).[14,15] To explore less characterized but biologically relevant candidates, we prioritized *A. putredinis* and *B. eggerthii*, which demonstrated significant reductions in both MASLD and obesity groups, warranting further experimental investigation. Although we successfully obtained *A. putredinis* (KGMB02772) and *B. eggerthii* (JCM 12986), repeated anaerobic culture attempts for *A. putredinis* failed due to complete loss of viability, a technical limitation commonly reported for *Alistipes* species. In contrast, *B. eggerthii* exhibited stable anaerobic growth, enabling subsequent functional validation in the WD–induced MASLD model. These findings collectively support the rationale for selecting *B. eggerthii* as the most suitable candidate for mechanistic investigation among the taxa depleted in MASLD.

Oral administration of *B. eggerthii* improves body weight, fat accumulation, and liver morphology in the MASLD mouse model

Figure 2A (left panel) shows the animal experimental design for evaluating *B. eggerthii* in MASLD and obese mice. The normal diet (ND) group represented the ND cohort, whereas the WD+PBS group was fed a WD and received oral administration of distilled water. The WD+B group was fed a WD and received oral administration of *B. eggerthii*. The WD consisted of 42.7% carbohydrates, 42% fat, and 15% protein and was administered for 12 weeks. Over time, the WD group exhibited the greatest increase in body weight, whereas the WD+B group showed statistically significant improvements in body weight and liver-to-body weight ratio (%) compared to the WD group (Fig. 2A, middle panel).

Examination of the abdominal cavity revealed that the WD+B group had reduced fat levels, resembling those of the ND group (Fig. 2A, right panel and 2B, top panel). A key characteristic feature of MASLD is liver whitening and enlargement. Representative liver images from each group showed that the WD group exhibited an enlarged and whitish liver, whereas the WD+B group displayed a liver size and color similar to that of the ND group (Fig. 2B, bottom panel).

Histological analysis of H&E-stained liver sections revealed a significant accumulation of lipid droplets in the WD group, whereas fat accumulation was markedly reduced in the WD+B group (Fig. 2C, top panel). IHC staining for Sirius red (collagen), CD68, and α-SMA demonstrated that *B. eggerthii* administration reduced collagen deposition, α-SMA expression, and lipid accumulation in the liver (Fig. 2C, bottom panel and 2D). Masson's trichrome (M&T) staining was used to assess the NAS and fibrosis. NAS significantly increased in the WD group; however, this trend was mitigated in the WD+B group (Fig. 2E, left panel). Fibrosis grading revealed varying stages (1a, 1b, and 2) in the WD group, whereas fibrosis severity was reduced to stages 1a and 1b in the WD+B group (Fig. 2E, right panel).

Serum biochemical tests were conducted to evaluate the liver function (Fig. 2F). The WD group exhibited increased serum ALT, AST, total bilirubin, cholesterol, triglycerides, and LDL-cholesterol levels, whereas they were significantly

https://doi.org/10.3350/cmh.2025.0475

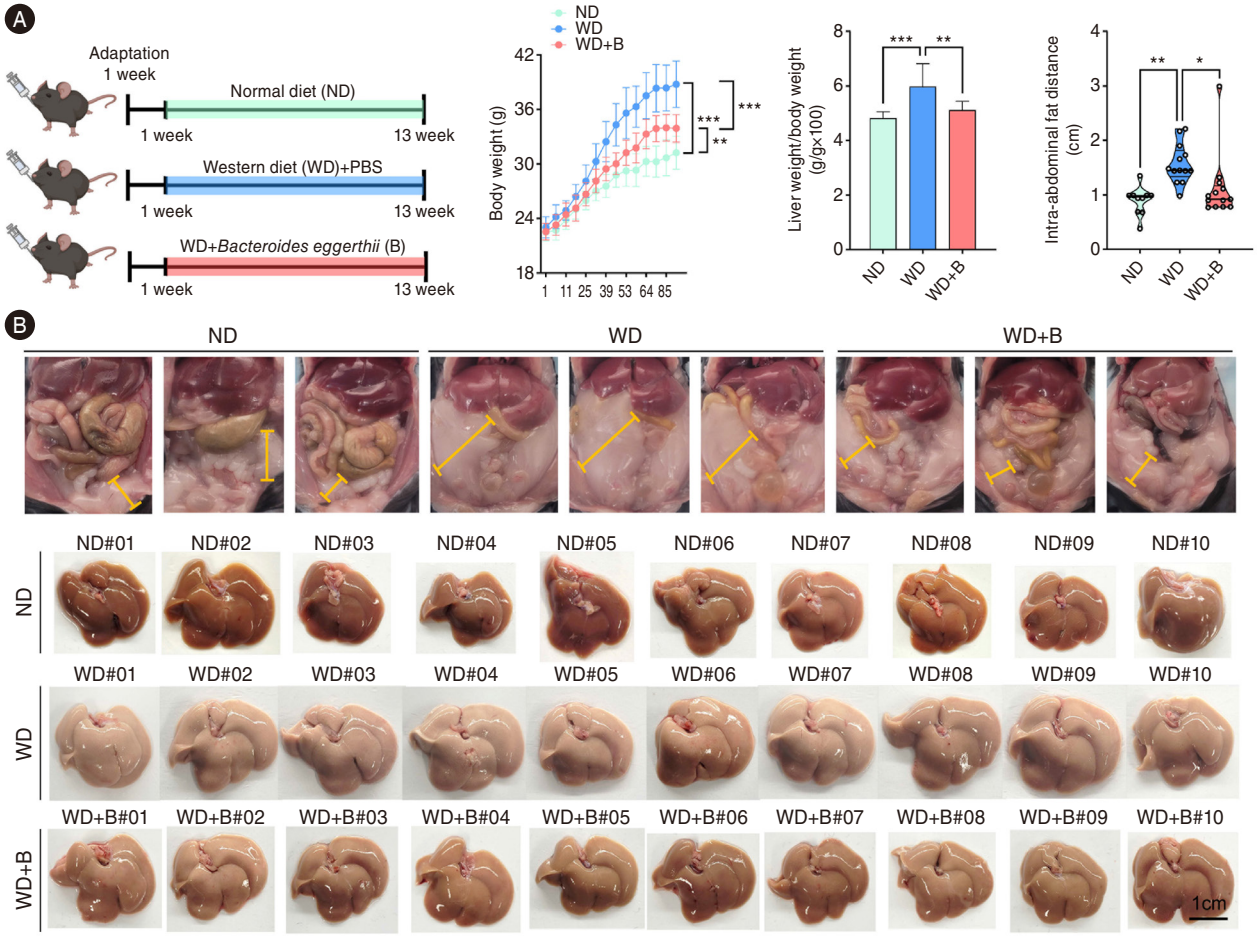

Figure 2. Effects of *Bacteroides eggerthii* on body weight, fat accumulation, and liver morphology in the metabolic dysfunction-associated steatotic liver disease (MASLD) mouse model. (A) Experimental design and gross phenotypic outcomes. Left: Experimental design for *B. eggerthii* administration in the MASLD mouse model. Middle: Body weight progression and liver-to-body weight ratio in normal diet (ND), Western diet (WD), and WD supplemented with *B. eggerthii* (WD+B) groups over 12 weeks. Right: Quantification of abdominal fat area, showing reduced fat accumulation in the WD+B group. (B) Liver morphology and gross features. Top: Representative images of abdominal fat deposits in each group, showing reduced fat accumulation in the WD+B group. Bottom: Gross morphology of livers, with whitening and enlargement observed in WD, alleviated in WD+B. Hematoxylin and eosin (H&E) staining of liver sections showed marked lipid droplet accumulation in WD, with reductions in WD+B. (C) Histological and fibrosis assessment. Top: H&E staining of liver sections, shows lipid droplet accumulation in WD, with marked reductions in WD+B. Bottom: Immunohistochemistry analysis for Sirius red (collagen), CD68, and α-SMA, indicate decreased fibrosis and collagen deposition in WD+B. (D) Quantitative comparison of collagen deposition, CD68-positive macrophages, and α-SMA expression among ND, WD, and WD+B groups, supporting the histological improvements observed in Panel C. (E) Masson's trichrome staining and nonalcoholic fatty liver disease activity score (NAS) evaluation, showing reduced fibrosis in the WD+B group. (F) Serum biochemical analysis demonstrates improved liver function in WD+B based on alanine aminotransferase (ALT), aspartate aminotransferase (AST), total bilirubin, cholesterol, triglyceride, and low-density lipoprotein (LDL)-cholesterol levels.

reduced in the WD+B group, indicating substantial liver function improvement.

Reconfiguration of gut microbiota and functional shifts induced by *B. eggerthii* in MASLD mice

To evaluate the effects of *B. eggerthii* on the gut microbiota composition, 16S rRNA sequencing was performed to compare the relative abundance of gut microbial taxa at the genus and species levels across the ND, WD, and WD+B groups. At the genus level, 15 taxa exhibited significant differences among groups, whereas at the species level, 19 differentially abundant taxa were identified (Fig. 3A).

Alpha diversity analyses, including ACE, Chao1, OTU count, and Shannon indices, did not reveal significant differ-

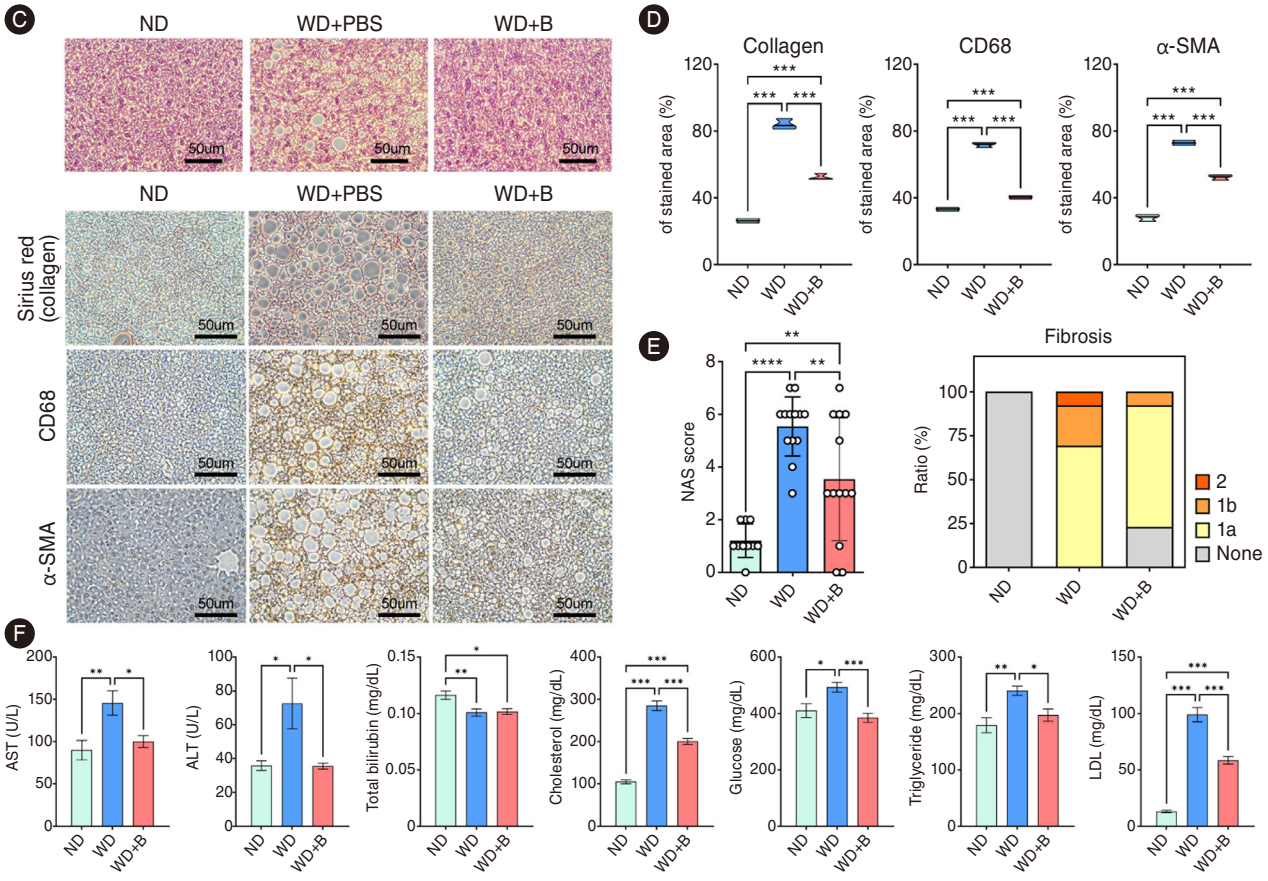

Figure 2. Continued.

ences between the WD and WD+B groups (Fig. 3B). However, beta diversity analysis using PCoA demonstrated clear segregation in response to dietary intervention and *B. eggerthii* administration (R^2=0.588, F=6.42, *P*=0.001) (Fig. 3C).

To investigate the functional implications of the observed microbial alterations, LEfSe analysis was performed using the PICRUSt dataset. Functional orthology analysis predicted a significant enrichment of 'choloylglycine hydrolase' in the WD+B group (Fig. 3D, left panel), while pathway analysis predicted 'microbial metabolism in diverse environments' and 'ribosome' (Fig. 3D, right panel). These computational predictions suggest that the prominently identified 'choloylglycine hydrolase' may play a role in bile acid metabolism, potentially contributing to the observed metabolic improvements following *B. eggerthii.*

To further support the functional relevance of *B. eggerthii*, we verified whether the administered strain could colonize the host gut. Using colonic tissue DNA, we performed strain-specific quantitative PCR (qPCR) targeting the *gyrB* gene of *B. eggerthii* (strain JCM12986). The results revealed a progressive increase in *B. eggerthii* signal across groups, with the highest abundance detected in the WD+B group compared to the WD group, indicating successful engraftment and persistence of the administered strain (Fig. 3E).

These findings provide molecular-level evidence that *B. eggerthii* not only persists in the gut environment after oral administration but also likely contributes to bile acid metabolism via enhanced choloylglycine hydrolase activity.

B. eggerthii modulates hepatic RNA transcription and metabolic pathways

To investigate the molecular mechanisms underlying *B. eggerthii*-mediated regulation, we analyzed hepatic transcriptomes across ND, WD, and WD+B groups. Heatmap analysis revealed distinct expression patterns, and 17 shared DEGs were identified across comparisons (ND vs.

https://doi.org/10.3350/cmh.2025.0475

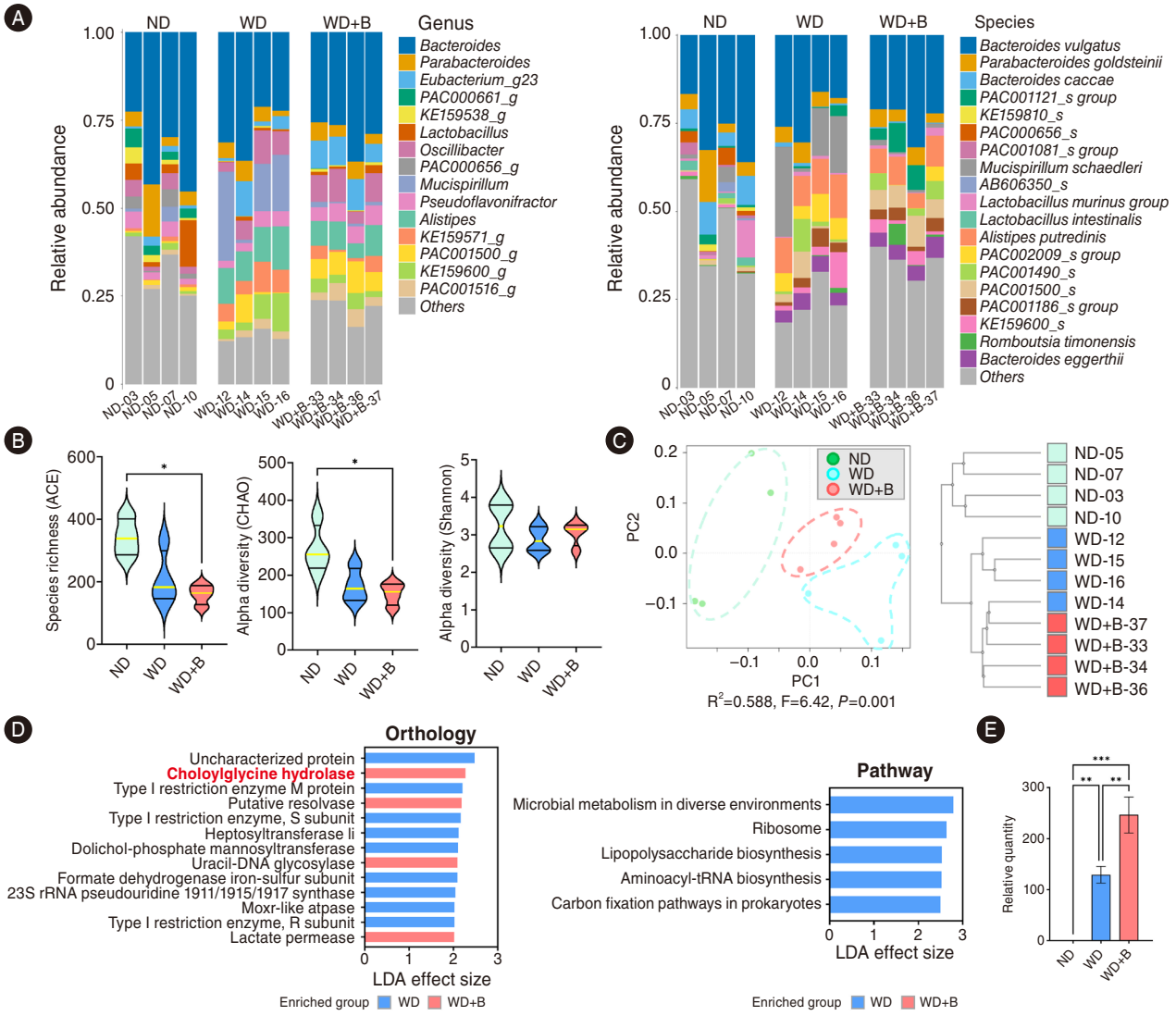

Figure 3. Gut microbiota composition and functional shifts following *Bacteroides eggerthii* administration. (A) Relative abundances of gut microbiota at the genus and species levels, with significant changes observed in Western diet (WD)+B compared to WD. (B) Alpha diversity indices (ACE, Chao1, OTU count, Shannon index), showing no significant difference between WD and WD+B groups. (C) Principal coordinates analysis (PCoA) and hierarchical clustering based on Bray–Curtis dissimilarity of fecal microbiota composition. PCoA plot shows distinct clustering among normal diet (ND, green), WD (cyan), and WD+B.E. (pink) groups. Dashed ellipses represent 95% confidence intervals. PERMANOVA analysis confirmed significant differences in microbial community composition across groups (R^2=0.588, F=6.42, *P*=0.001). Right panel shows hierarchical clustering dendrogram of the top five most abundant taxa per group. (D) Linear discriminant analysis effect size (LEfSe) analysis based on the PICRUSt functional prediction, showing enrichment of choloylglycine hydrolase in the WD+B group, along with predicted enrichment of microbial metabolism in diverse environments and ribosome function. (E) Strain-specific quantitative polymerase chain reaction (qPCR) analysis of *B. eggerthii* in mouse colon tissue. Colonic DNA was subjected to qPCR using primers specific for the *gyrB* gene of *B. eggerthii*. The relative abundance of *B. eggerthii* was normalized to total bacterial 16S rRNA levels. Data represent mean±standard error of the mean. Statistically significant differences were determined using one-way analysis of variance (ANOVA) with Tukey's *post-hoc* test; ***P*<0.01, ****P*<0.001.

WD, WD vs. WD+B) (Fig. 4A). These genes were altered by WD feeding but partially or fully restored with *B. eggerthii* treatment, and enrichment analysis linked them to fatty acid metabolism, bile acid homeostasis, and PPAR signaling (Supplementary Fig. 1). GSEA was performed to identify enriched gene sets in each group. In the ND vs. WD comparison, the WD group showed significant FATTY_ACID_METABOLISM enrichment, whereas the ND group

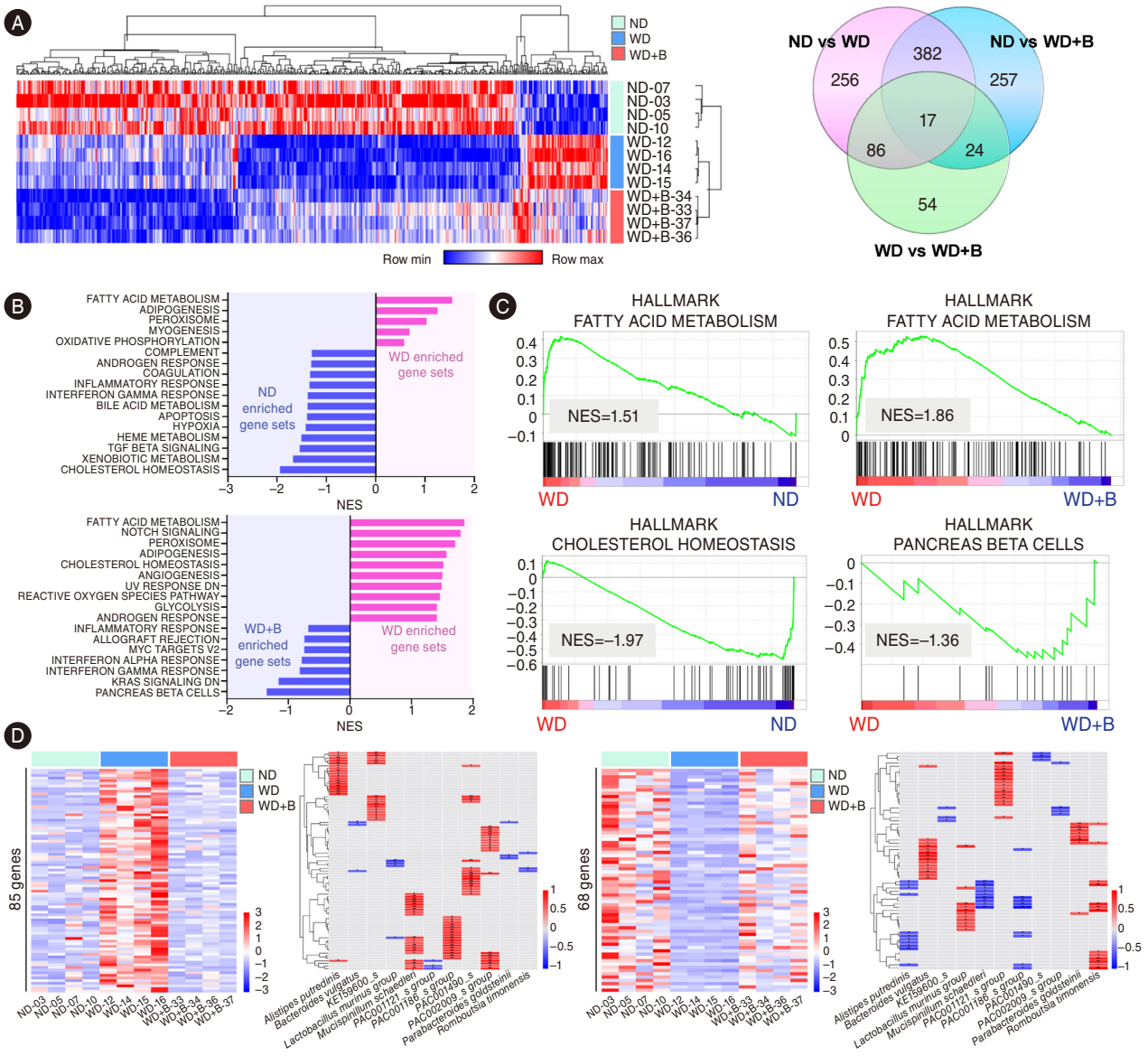

Figure 4. Transcriptomic changes in the liver following *Bacteroides eggerthii* intervention. (A) Left: Heatmap analysis of differentially expressed genes across the normal diet (ND), Western diet (WD), and WD+B groups, shows a distinct transcriptional profile in WD+B. Right: Venn diagram illustrating 17 commonly altered genes across all groups. (B) Gene Set Enrichment Analysis (GSEA) comparing ND vs. WD groups. Top: Significant enrichment of FATTY_ACID_METABOLISM in WD and CHOLESTEROL_HOMEOSTASIS in ND. Bottom: PANCREAS_BETA_CELLS enrichment in WD+B suggests partial metabolic restoration. (C) Representative GSEA plots highlighting key metabolic pathways restored in WD+B, including reduced fatty acid metabolism and restored cholesterol homeostasis. (D) Heatmaps of gene subsets reversed by *B. eggerthii* intervention. Left: 85 genes upregulated in WD and downregulated in WD+B. Right: 68 genes downregulated in WD and upregulated in WD+B. (E) Gene Ontology (GO) enrichment analysis of altered gene sets, linking fatty acid metabolism and immune responses to MASLD progression and *B. eggerthii* intervention. (F) RNA-seq and quantitative real-time polymerase chain reaction analyses of hepatic genes involved in fatty acid metabolism (*Pparg*, *Cd36*, *Fabp1*) and bile acid metabolism (*Nr1h4*, *Cyp8b1*) in ND, WD, and WD+B groups. (G) Western blot analysis of FXR and CD36 proteins in liver tissue (left), and FXR, FGF15, and CYP8B1 in ileal tissue (right). Densitometric quantification was performed using GAPDH as a loading control. Data are presented as mean±standard error of the mean. Statistical significance was determined using one-way ANOVA with Tukey's *post-hoc* test. **P*<0.05, ***P*<0.01, ****P*<0.001.

showed CHOLESTEROL_HOMEOSTASIS enrichment (Fig. 4B, top panel). Similarly, in the WD+B vs. WD comparison, WD remained enriched for FATTY_ACID_METABOLISM, whereas the WD+B group was significantly enriched for PANCREAS_BETA_CELLS (Fig. 4B, bottom panel). GSEA plots further illustrate these trends: FATTY_

https://doi.org/10.3350/cmh.2025.0475

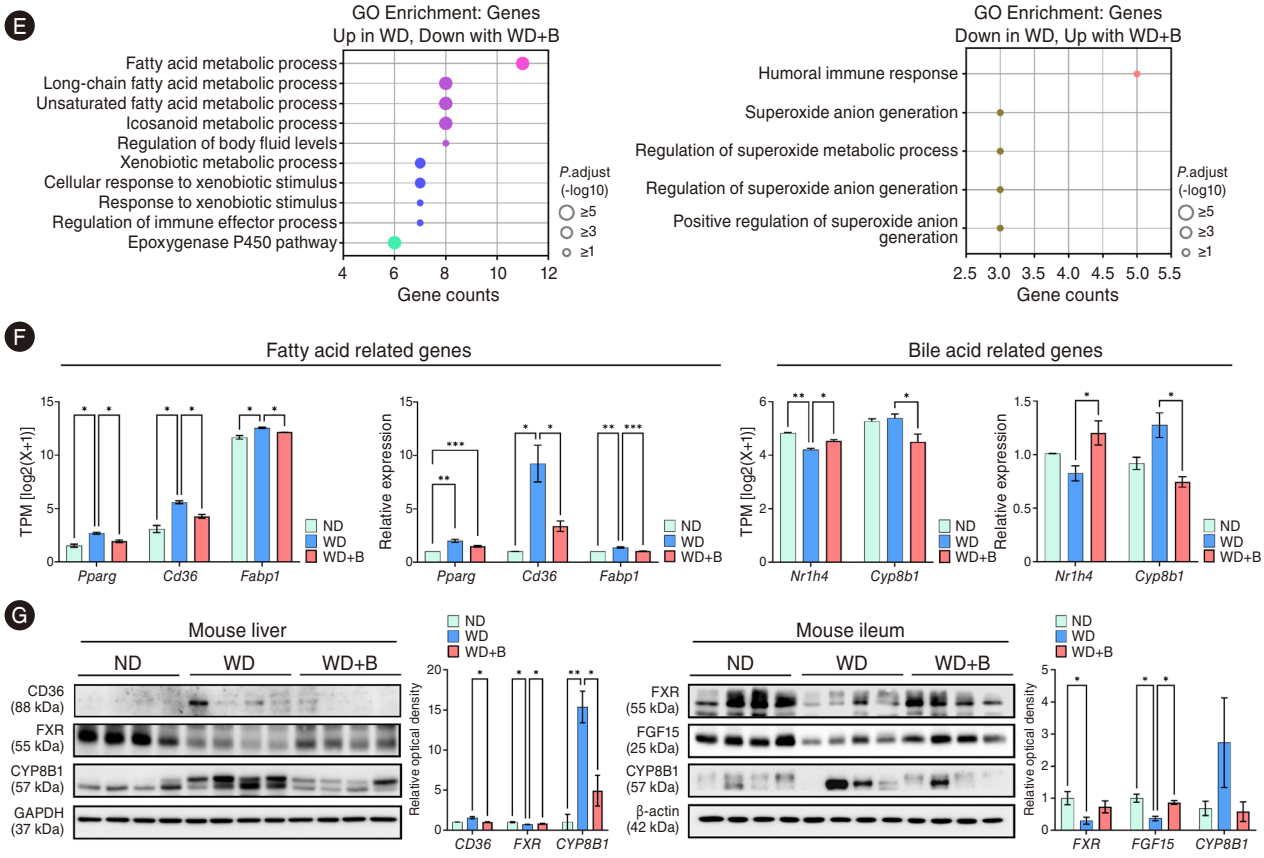

Figure 4. Continued.

ACID_METABOLISM was positively enriched in WD relative to ND (NES=1.51) and also in WD compared to WD+B (NES=1.86). Conversely, CHOLESTEROL_HOMEOSTASIS was enriched in ND relative to WD (NES=–1.97), whereas PANCREAS_BETA_CELLS was enriched in WD+B compared to WD (NES=–1.36) (Fig. 4C). These results highlight the metabolic shifts induced by WD and suggest that *B. eggerthii* administration may contribute to metabolic restoration by reversing disease-associated transcriptional changes.

We further examined the gene expression patterns modulated by *B. eggerthii*. In total, 85 genes were significantly upregulated in the WD group compared to those in ND group, and their expression was subsequently downregulated in WD+B group (Fig. 4D, left panel). Correlation heatmap analysis indicated that most genes were strongly positively correlated with microbial taxa (Fig. 4D, left panel). Conversely, 68 genes were downregulated in WD compared to ND, but their expression was restored in WD+B group (Fig. 4D, right panel). Correlation analysis revealed decreased positive correlations and increased negative correlations among the 68 genes in response to *B. eggerthii* (Fig. 4D, right panel).

Gene Ontology enrichment analysis was performed to functionally categorize transcriptomic changes. The 85 genes upregulated in WD and downregulated in WD+B exhibited the highest enrichment in the fatty acid metabolic process, which aligns with the transcriptomic findings (Fig. 4E, left panel). In contrast, the 68 downregulated genes in WD with subsequent upregulation in WD+B were primarily associated with humoral immune response (Fig. 4E, right panel).

To validate these findings, we examined the expression patterns of host hepatic genes related to fatty acid and bile acid metabolism following *B. eggerthii* administration. As shown in Figure 4F (left panel), qRT-PCR analysis revealed that the mRNA levels of key lipid metabolism–related genes —*Pparg*, *Cd36*, *and Fabp1*—were significantly ele-

 https://doi.org/10.3350/cmh.2025.0475

vated in WD-fed mice compared to ND, indicating hepatic lipid accumulation. These aberrant elevations were markedly attenuated in the WD+B group, consistent with the reversal of steatotic changes. In contrast, expression of Nr1h4 (FXR), a central nuclear receptor involved in bile acid and lipid metabolism, was suppressed in WD-fed mice but significantly restored in the WD+B group. Western blot analysis confirmed these transcript-level changes at the protein level (Fig. 4F, right panel), showing that CD36 protein was increased in WD but normalized in WD+B, whereas FXR protein was decreased in WD and restored upon *B. eggerthii* administration.

We next explored FXR-related downstream signaling in both liver and intestine. Hepatic expression of CYP8B1, a key enzyme that controls bile acid composition and is negatively regulated by FXR, was significantly increased in WD-fed mice but reduced in the WD+B group at protein levels (Fig. 4G, left). Furthermore, intestinal FXR–FGF15 axis was evaluated. In the ileum, the expression of FXR and its downstream effector FGF15 was decreased in WD-fed mice, consistent with impaired intestinal FXR signaling. Notably, both targets were upregulated in the WD+B group, suggesting that *B. eggerthii* restored intestinal FXR pathway activity. Intestinal CYP8B1 levels, which were elevated in WD-fed mice, were also reduced in parallel upon *B. eggerthii* treatment (Fig. 4G, right).

These results collectively suggest that *B. eggerthii* administration reactivates the hepatic and intestinal FXR pathways, leading to the normalization of lipid and bile acid metabolic regulators. This multi-level restoration likely contributes to the observed attenuation of WD-induced hepatic steatosis and metabolic dysfunction. Using an external publicly available human liver tissue RNA-seq dataset (GSE135251), pathway enrichment analysis revealed significant enrichment of MASLD-relevant pathways, including fatty acid metabolism, cholesterol regulation, and inflammatory responses, which closely aligned with the transcriptomic signatures observed in our mouse model (Supplementary Fig. 2).

Metabolomic alterations induced by *B. eggerthii* and network-based analysis of metabolite-microbiome interactions

To elucidate the metabolic changes induced by *B. eggerthii*, we conducted fecal metabolite profiling across ND, WD, and WD+B groups using GC-TOF-MS and UHPLC-LTQ-Orbitrap-MS/MS. Metabolomic analyses revealed distinct clustering among the three groups, highlighting significant shifts in fecal metabolite composition following WD and *B. eggerthii* intervention (Fig. 5A). Via GC-TOF-MS, 21 metabolites were identified, whereas 10 bile acids were detected using UHPLC-LTQ-Orbitrap-MS/MS. These metabolites included 17 fatty acids, two carbohydrates, and two additional metabolites. Most metabolites and bile acids were significantly elevated in the WD group compared to those in the ND group, whereas WD+B administration led to partial restoration of ND levels (Fig. 5B).

ROC curve analysis was performed to evaluate the diagnostic potential of specific metabolites. Among the five most distinguishing metabolites that differentiated ND and WD+B from WD, 1-pentadecanol exhibited the highest AUC value (0.90), suggesting its potential as liver-associated metabolic features (Fig. 5C, left panel). Similarly, 7-sulfocholic acid, one of the five significantly altered bile acids, demonstrated the highest AUC value (0.90), reinforcing its potential role as a biomarker of bile acid metabolism (Fig. 5C, right panel). To confirm the robustness of these ROC results, we further calculated 95% confidence intervals using bootstrap and DeLong methods, and performed stratified cross-validation with FDR-adjusted pairwise comparisons. These analyses consistently supported the reliability of the findings, as detailed in Supplementary Tables 3 and 4.

To further explore the metabolite-microbiome interactions, network analysis was conducted to assess the associations between microbial taxa and fecal metabolites in the WD+B group (Fig. 5D). The PAC001186 group exhibited strong associations with key bile acids, including deoxycholic, cholic, and taurodeoxycholic acids, suggesting its functional role in bile acid metabolism. Additionally, KE159600_s was closely linked to bile acid transformation pathways. The PAC002009_s group showed extensive correlations with multiple bile acids such as 3-oxocholic and tauro-ursodeoxycholic acids, underscoring its significant contribution to bile acid metabolism. Moreover, *A. putredinis* displayed robust associations with cholic and chenodeoxycholic acids, emphasizing its pivotal role in bile acid modification and microbial-metabolite interactions.

These findings highlight the profound impact of *B. eggerthii* on host metabolism, particularly on bile acid transfor-

https://doi.org/10.3350/cmh.2025.0475

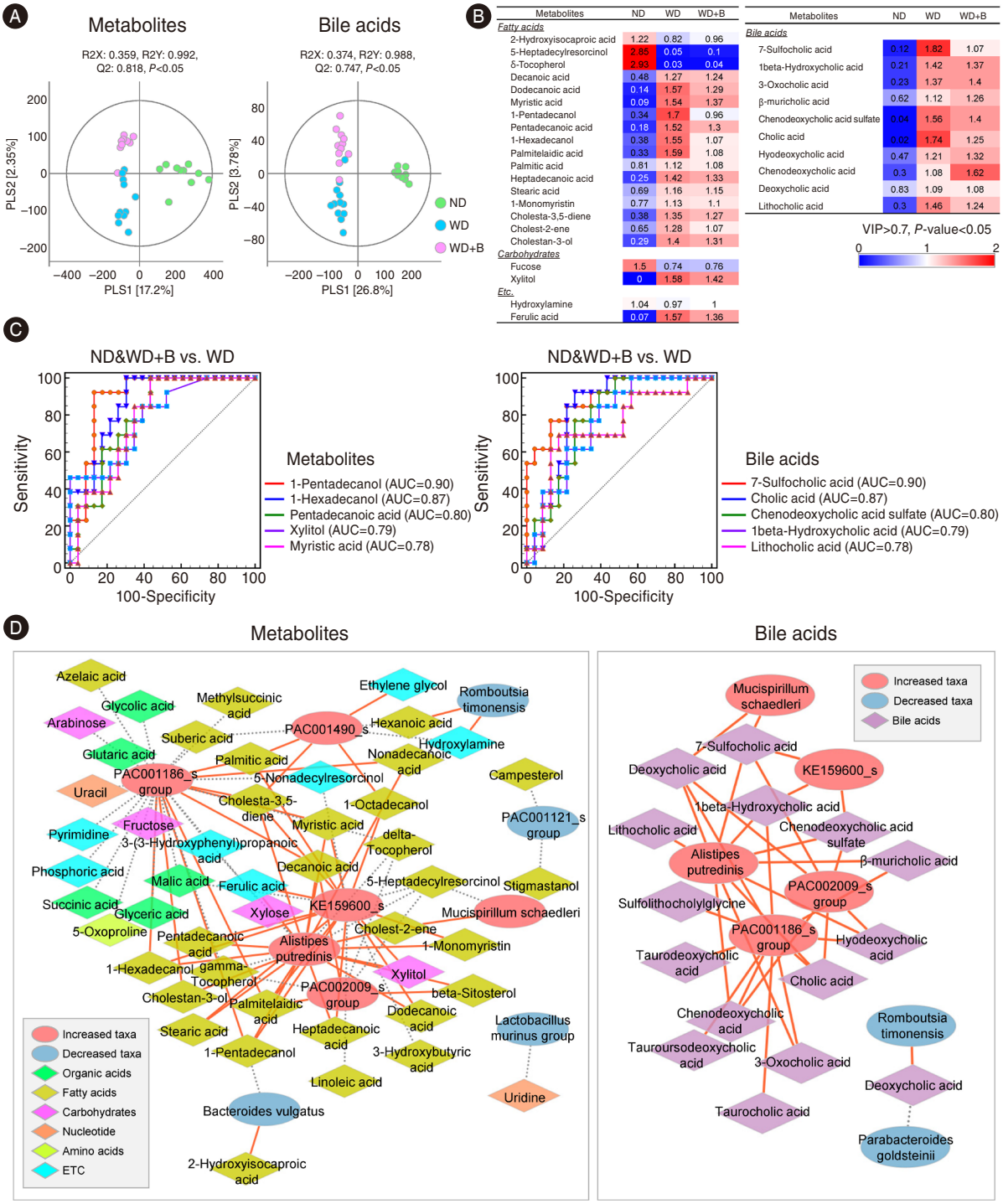

Figure 5. Metabolomic alterations induced by *Bacteroides eggerthii* and network-based analysis of metabolite-microbiome interactions. (A) Principal coordinates analysis analysis of fecal metabolomic profiles demonstrates distinct clustering among normal diet (ND), Western diet (WD), and WD+B groups. Green circles represent the ND group, blue circles represent the WD group, and pink circles represent the WD+B (*B. eggerthii*) group. (B) Heatmap of significantly altered metabolites, highlighting increased bile acid and lipid metabolites in WD compared to ND, with partial restoration in WD+B. (C) Receiver operating characteristic curve analysis of differentially abundant metabolites (ND and WD+B vs. WD), identifying 1-pentadecanol (area under the curve [AUC]=0.90) and 7-sulfocholic acid (AUC=0.90) as liver-associated metabolic features of *B. eggerthii* treatment. (D) Interaction network depicting associations between microbial taxa and fecal metabolites in the WD+B group. Nodes represent microbial taxa (ovals) and metabolites (diamonds, hexagons, or other shapes), with bile acids indicated in purple. Edges represent significant correlations.

mation and fatty acid regulation, suggesting its potential therapeutic role in modulating metabolic imbalances associated with MASLD.

B. eggerthii-derived 2-hydroxyisocaproic acid restoration and its anti-steatotic role

From the mouse fecal metabolomic profiles (GC-TOF-MS and UHPLC-LTQ-Orbitrap-MS/MS), 2-hydroxyisocaproic acid (HICA) was identified as a metabolite of interest based on its distinct regulation across groups: it decreased in the WD group (relative intensity: 0.82) compared to the ND group (1.22), but was modestly restored in the WD+B group (0.96) (Fig. 5B). To confirm that HICA is directly produced by *B. eggerthii*, we analyzed its culture medium and observed a substantial elevation in HICA concentration in the *B. eggerthii*-conditioned medium (relative intensity: 1.91) compared to the control medium (0.09), strongly suggesting microbial origin (Fig. 6A, 6B). We further validated these findings through statistical comparisons. In fecal samples, HICA levels were significantly reduced in the WD group versus the ND group, and significantly increased again in the WD+B group ($P<0.05$, one-way ANOVA with Tukey's *post-hoc* test). Similarly, in the *in vitro* analysis, HICA levels were significantly higher in the *B. eggerthii*-conditioned medium compared to control ($P<0.001$, unpaired *t*-test), confirming that oral administration of *B. eggerthii* restores HICA *in vivo* (Fig. 6C). To further evaluate HICA's functional role, we established an *in vitro* steatosis model using HepG2 and Hepa1-6 cells. First, MTT assays confirmed that HICA was non-toxic across all concentrations tested (Fig. 6D). Next, we assessed intracellular lipid accumulation using Oil Red O staining, along with cell viability measurements. The results of both assays were that HICA treatment attenuated lipid accumulation in a dose-dependent manner, especially under free fatty acid-induced steatotic conditions (Fig. 6E, 6F). These findings support the hypothesis that HICA contributes to the anti-steatotic effects of *B. eggerthii*, at least in part, by modulating hepatic lipid metabolism (Fig. 6G).

DISCUSSION

Recent evidence has demonstrated the significant role of the gut microbiota in the pathogenesis of MASLD, showing that gut dysbiosis contributes to liver lesions such as steatosis, metabolic dysfunction-associated steatohepatitis, fibrosis, and liver cancer in animal models.[16] Despite these insights, few studies have analyzed human data. Our study bridges this gap by identifying potentially beneficial gut bacterial candidates in humans with MASLD and validating their therapeutic effects using mouse model experiments. This study compared the gut microbiome composition of patients with MASLD and healthy controls, confirming *B. eggerthii* reduction in both the MASLD and obesity groups. In a mouse model in which MASLD was induced by a WD, oral *B. eggerthii* administration significantly improved body weight, liver weight, and liver histology. Furthermore, we employed an integrative multi-omics approach—including microbiome, fecal metabolomics, and transcriptomics (liver and intestine)—to elucidate the microbial–host metabolic interaction. Using strain-specific qPCR, we demonstrated enhanced colonization of *B. eggerthii* in the colon of WD+B mice. Through transcriptomic analysis (qRT-PCR and Western blot), we confirmed regulation of key lipid and bile acid–related genes (e.g., CD36, FABP1, PPARG, FXR, CYP8B1, FGF15) at the transcript and/or protein levels. Notably, untargeted metabolomics revealed 2-hydroxyisocaproic acid (HICA) as a commonly upregulated metabolite in both *B. eggerthii* culture supernatants and fecal samples from treated mice. We further demonstrated that HICA exerts anti-steatotic effects in FFA-induced steatosis models using both HepG2 and Hepa1-6 cells—representing, to our knowledge, the first functional validation of this metabolite in this context.

Recent evidence highlights distinct gut microbiome changes associated with MASLD. Specific bacterial signatures exhibited by patients differentiate early from advanced fibrosis, and are characterized by increased *Proteobacteria* and *Escherichia coli* abundance and concurrent *Firmicutes* and *Faecalibacterium prausnitzii* decrease.[17] Additionally, gut microbiome profiles can distinguish cirrhotic from non-cirrhotic individuals, regardless of disease etiology or geographic location.[18] Hepatic steatosis is linked to reduced microbial diversity and *Coprococcus* and *R. gnavus* presence.[19] A study in Germany demonstrated that long-term gut microbiome instability dominated by *Enterobacteriaceae* and *Escherichia*/*Shigella* correlates with MASLD and type 2 diabetes progression.[20] Furthermore, *Akkermansia muciniphila* has emerged as a benefi-

https://doi.org/10.3350/cmh.2025.0475

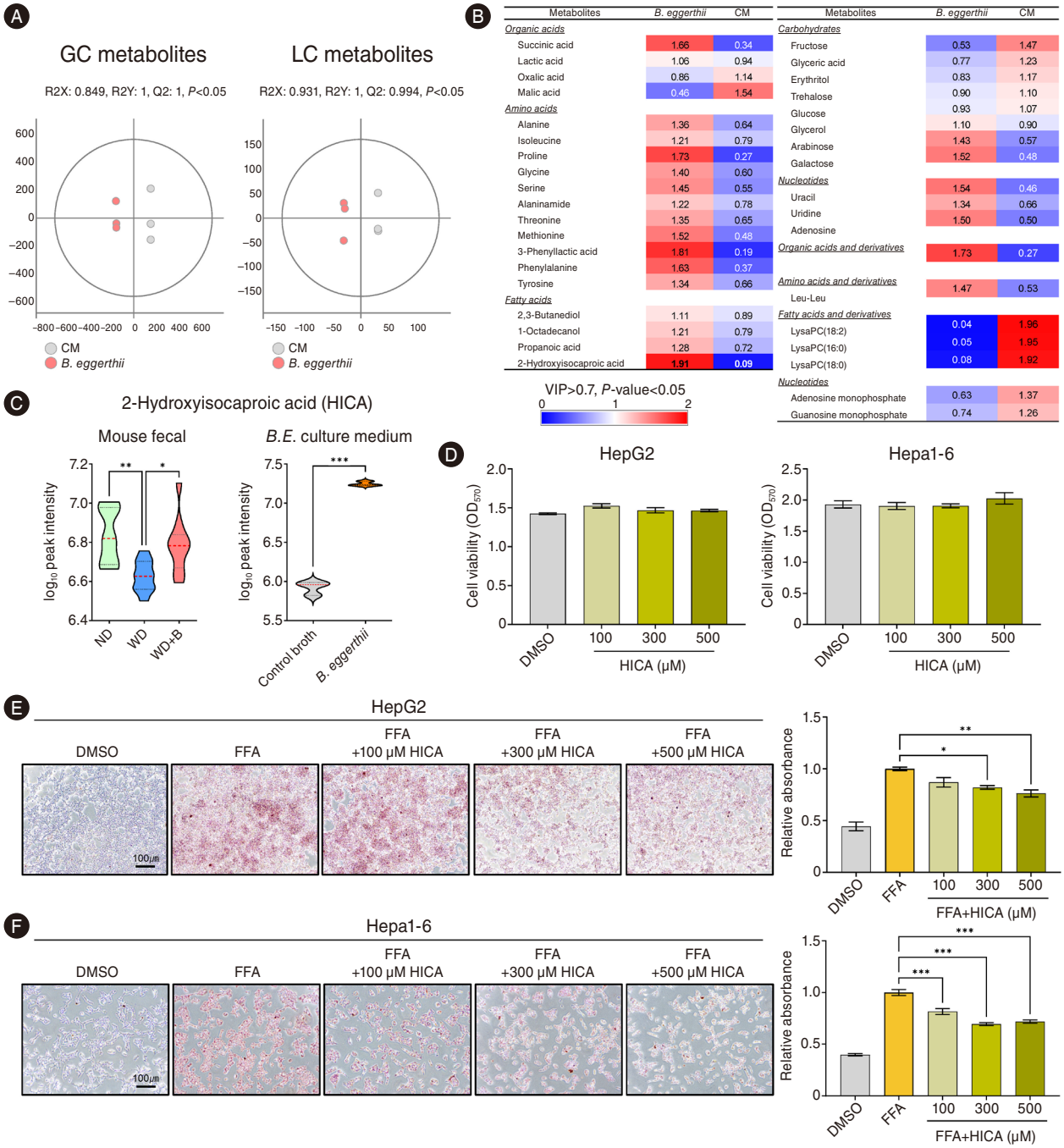

Figure 6. *Bacteroides eggerthii*-derived 2-hydroxyisocaproic acid (HICA) restoration and its anti-steatotic role. (A) PLS-DA score plots of fecal metabolomic profiles obtained by GC-TOF-MS and UHPLC-LTQ-Orbitrap-MS/MS, demonstrating distinct clustering between control and *B. eggerthii*–treated groups. (B) Heatmap of discriminant metabolites (VIP>0.7, $P<0.05$) in the *B. eggerthii*-conditioned medium and the control medium, highlighting HICA as a key metabolite modulated by *B. eggerthii*. (C) Relative intensity of HICA in mouse fecal samples (normal diet [ND], Western diet [WD], and WD+*B. eggerthii* groups) and *in vitro* culture medium, showing reduced HICA levels under WD, restoration with *B. eggerthii* administration, and direct production by *B. eggerthii* (***$P<0.001$, one-way ANOVA with Tukey's *post-hoc* test; unpaired *t*-test). (D) MTT assays confirming no cytotoxicity of HICA at concentrations up to 500 μM in HepG2 and Hepa1-6 cells. (E, F) Oil Red O staining and quantification in HepG2 and Hepa1-6 cells demonstrating that HICA treatment attenuates free fatty acid-induced lipid accumulation in a dose-dependent manner. *$P<0.05$, **$P<0.01$, ***$P<0.001$. (G) Schematic illustration summarizing the mechanism: *B. eggerthii* produces HICA, which reduces hepatic lipid accumulation and exerts anti-steatotic effects. Data are presented as mean±standard error of the mean. Statistical significance was determined by one-way ANOVA with Tukey's *post-hoc* test (panels C, left, E, F) or unpaired *t*-test (panel C, right).

 https://doi.org/10.3350/cmh.2025.0475

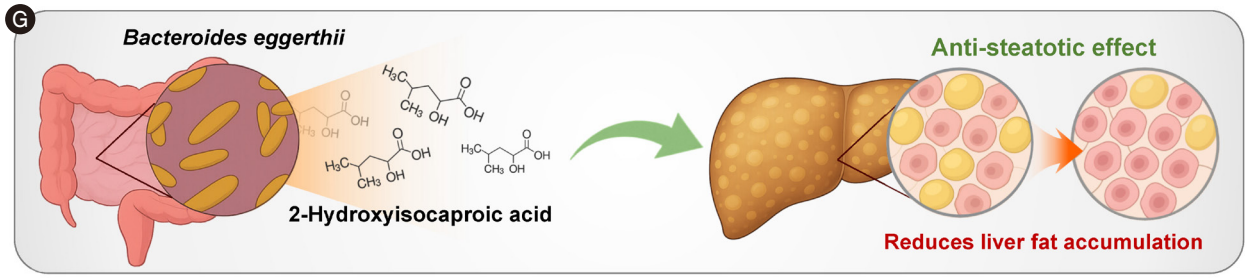

Figure 6. Continued.

cial bacterium with antiobesogenic benefits, improving metabolic parameters in humans with obesity, and the membrane protein Amuc-110 contributes to these effects.[21] These findings underscore the critical role of gut microbiota in MASLD pathogenesis and highlight the potential of microbiome-based therapeutic interventions.

Three reports exist on changes in *B. eggerthii* in MASLD or obesity. A recent study analyzed the stool metagenomes of >870 individuals from five countries and identified 42 microbiome species capable of distinguishing between obese and healthy individuals. In this study, decreased *B. eggerthii* occurred in the obesity group and is proposed as a beneficial broad-spectrum target alongside *A. muciniphila*, *F. prausnitzii*, *Prevotella copri*, *B. dorei*, *Alistipes finegoldii*, *A. shahii*, *Eubacterium* sp. CAG_180, and *Roseburia hominis*.[22] Conversely, among children with obesity, increased *B. eggerthii* occurred compared to that in normal-weight Mexican children.[23] Another study analyzing the gut microbiome of 78 obese and 25 eutrophic individuals found increased *B. eggerthii* in the obesity group, presenting contradictory findings to ours.[24] However, all three studies performed microbiome analyses alone, without functional investigations using animal experiments, to determine *B. eggerthii* effects on MASLD or obesity. In contrast, our study integrated human stool sample analysis with animal experiments and multi-omics data analysis, providing a more comprehensive understanding of *B. eggerthii* roles in MASLD and obesity.

We conducted metagenomic and metabolomic analyses using mouse fecal samples and transcriptomic analysis using mouse liver tissues to investigate how *B. eggerthii* improves MASLD. Notably, although *B. eggerthii* abundance did not significantly increase in the WD+B group, LEfSe analysis of PICRUSt-predicted functions indicated significant enrichment of the orthologous group annotated as 'choloylglycine hydrolase. Although direct evidence linking *B. eggerthii* to bile acid metabolism is limited, other species within the B. genus play critical roles in bile acid deconjugation and transformation. For instance, *B. thetaiotaomicron* contributes to primary bile acids conversion into secondary bile acids via bile salt hydrolase activity.[25] Our study also observed bile acid profile changes through mouse fecal metabolite analysis. Western blot analysis of mouse liver tissues revealed increased FXR expression, which decreased in the WD group, after *B. eggerthii* treatment. This finding suggests that *B. eggerthii* contributes to bile acid metabolism, leading to MASLD improvement. However, we acknowledge that we did not include direct *in vitro* assays of bile salt hydrolase activity or targeted bile-acid profiling. Therefore, we suggest that the PICRUSt-derived functional predictions be interpreted with caution.

To reconcile these abundance patterns with the observed protective effects, we note that fecal 16S data are inherently compositional. WD-associated shifts in *B. eggerthii* reflect relative abundance against a changing community baseline and do not quantify absolute load or mucosa-associated colonization. To address this, we performed strain-specific qPCR (gyrB) on colonic tissue and observed clear engraftment in WD+B but negligible signal in ND, indicating diet-dependent colonization of the administered strain. At the functional level, the WD+B group showed restoration of intestinal FXR–FGF15 signaling and repression of hepatic CYP8B1, and our metabolomics/culture experiments identified HICA as a *B. eggerthii*–derived metabolite with anti-steatotic activity *in vitro*. These mechanistic outputs explain why a higher relative abundance under WD is not incompatible with a beneficial role: endogenous *B. eggerthii* may remain below a functional threshold to counteract WD-driven pathology, whereas oral administration enhances effective colonization and effector output, leading

https://doi.org/10.3350/cmh.2025.0475

to improved liver outcomes.

To further investigate the functional relevance of HICA, we conducted *in vitro* experiments using fatty acid–induced steatosis models in HepG2 and Hepa1-6 cells. Co-treatment with HICA significantly reduced intracellular lipid accumulation in a dose-dependent manner, as assessed by Oil Red O staining. MTT assays confirmed that HICA was non-toxic across all tested concentrations. These findings support that HICA, a metabolite directly produced by *B. eggerthii*, contributes to the anti-steatotic effects observed *in vivo* by modulating hepatic lipid metabolism. While our study focused primarily on experimental validation of HICA production and its anti-steatotic effects in FFA-induced steatosis models, previous literature supports HICA's broader biological functions. For instance, Nieminen et al.[26] reported that DL-2-hydroxyisocaproic acid attenuates inflammatory responses by reducing matrix metalloproteinase-9 (MMP-9) and myeloperoxidase (MPO) activity while preserving the expression of developmental endothelial locus-1 (Del-1) in a murine *Candida albicans* infection model, indicating its general tissue-protective and anti-inflammatory properties. Furthermore, HICA has been identified as a natural metabolite produced by lactic acid bacteria during kimchi fermentation. In this study, HICA levels increased significantly during fermentation and correlated with the expression of the HicD gene, highlighting its relevance to dietary intake and microbial ecology.[27] Additionally, a recent study identified a novel lipooligosaccharide structure produced by *B. eggerthii* that contains galactofuranose and shows weak immunostimulatory activity. This finding suggests that *B. eggerthii* may confer immunometabolic benefits through both structural and metabolic components, including HICA.[13] We believe these complementary lines of evidence collectively strengthen the biological plausibility and therapeutic potential of *B. eggerthii* and its metabolites in modulating host metabolism and inflammation.

Our study had several limitations. First, while the therapeutic potential of *B. eggerthii* is intriguing, we did not establish a direct mechanistic link between *B. eggerthii* and bile or fatty acid metabolism; thus, the current evidence remains largely correlative and should be interpreted with caution. In particular, although we demonstrated anti-steatotic effects of HICA, we did not establish a direct mechanistic connection between HICA and bile acid–related pathways, which should be addressed in future studies. Second, our experimental design did not include an ND+*B. eggerthii* group, which restricts our ability to determine whether the observed effects are specific to the pathological context of WD–induced MASLD or reflect broader physiological actions under normal conditions. Third, although *A. putredinis* was identified as another depleted strain in MASLD and initially considered for validation, it was excluded due to repeated culture failure under anaerobic conditions, a technical limitation commonly encountered in microbiome research. Fourth, although we expanded our validation of the FXR–FGF15–CYP8B1 pathway to include protein-level analyses, we acknowledge that additional FXR-independent mechanisms may contribute to the observed effects and were not fully explored. Fifth, the human microbiome dataset used for microbial feature selection was cross-sectional, which precludes causal inference and should be considered hypothesis-generating rather than confirmatory. Finally, we did not evaluate the safety, host specificity, or long-term colonization capacity of *B. eggerthii*, all of which are critical for its development as a therapeutic agent. Future studies incorporating safety assessments, host-specific responses, colonization tracking, and ultimately human clinical trials will be essential to rigorously establish the translational potential of *B. eggerthii*.

In conclusion, our findings demonstrate significant promise of *B. eggerthii* as a therapeutic target, and offer valuable insights into the development of microbiome-based strategies for treating and preventing MASLD.

Authors' contribution

SSK, JWE, and JYC contributed to conception and design. MGY, SHJ, GOB, HSJ, NL, CHL, and JC performed collected and assembled the data. JWE and JEH contributed to data analysis and interpretation. JC, MGY, JWE and SSK drafted the manuscript. All the authors have reviewed and approved the final manuscript. SSK is responsible for the overall content as guarantor.

Acknowledgements

The Biospecimens and data used in this study were provided by the Biobank of AJOU University Hospital, a member of Korea Biobank Network. This work was supported by the National Research Foundation of Korea (NRF) grant funded by the Korea government (MSIT) (RS-2025-

00521818, RS-2025-00562556, and RS-2022-NR070489) and a grant of the Korea Health Technology R&D Project through the Korea Health Industry Development Institute (KHIDI) funded by the Ministry of Health & Welfare, Republic of Korea (RS-2023-KH136690).

Data are available on reasonable request. Data are available on reasonable request by sending a message to the corresponding author.

Conflicts of Interest

The authors have no conflicts to disclose.

SUPPLEMENTARY MATERIAL

Supplementary material is available at Clinical and Molecular Hepatology website (http://www.e-cmh.org).

REFERENCES

1. Rinella ME, Lazarus JV, Ratziu V, Francque SM, Sanyal AJ, Kanwal F, et al. A multisociety Delphi consensus statement on new fatty liver disease nomenclature. J Hepatol 2023;79:1542-1556.
2. Friedman SL, Neuschwander-Tetri BA, Rinella M, Sanyal AJ. Mechanisms of NAFLD development and therapeutic strategies. Nat Med 2018;24:908-922.
3. Younossi ZM, Koenig AB, Abdelatif D, Fazel Y, Henry L, Wymer M. Global epidemiology of nonalcoholic fatty liver disease-meta-analytic assessment of prevalence, incidence, and outcomes. Hepatology 2016;64:73-84.
4. European Association for the Study of the Liver (EASL); European Association for the Study of Diabetes (EASD); European Association for the Study of Obesity (EASO). EASL-EASD-EASO Clinical Practice Guidelines on the management of metabolic dysfunction-associated steatotic liver disease (MASLD). J Hepatol 2024;81:492-542.
5. Kanwal F, Neuschwander-Tetri BA, Loomba R, Rinella ME. Metabolic dysfunction-associated steatotic liver disease: Update and impact of new nomenclature on the American Association for the Study of Liver Diseases practice guidance on nonalcoholic fatty liver disease. Hepatology 2024;79:1212-1219.
6. Tripathi A, Debelius J, Brenner DA, Karin M, Loomba R, Schnabl B, et al. The gut-liver axis and the intersection with the microbiome. Nat Rev Gastroenterol Hepatol 2018;15:397-411.
7. Turnbaugh PJ, Ley RE, Mahowald MA, Magrini V, Mardis ER, Gordon JI. An obesity-associated gut microbiome with increased capacity for energy harvest. Nature 2006;444:1027-1031.
8. Ley RE, Bäckhed F, Turnbaugh P, Lozupone CA, Knight RD, Gordon JI. Obesity alters gut microbial ecology. Proc Natl Acad Sci U S A 2005;102:11070-11075.
9. Cui C, Gao S, Shi J, Wang K. Gut-liver axis: the role of intestinal microbiota and their metabolites in the progression of metabolic dysfunction-associated steatotic liver disease. Gut Liver 2025;19:479-507.
10. Maher S, Rajapakse J, El-Omar E, Zekry A. Role of the gut microbiome in metabolic dysfunction-associated steatotic liver disease. Semin Liver Dis 2024;44:457-473.
11. Saeed H, Díaz LA, Gil-Gómez A, Burton J, Bajaj JS, Romero-Gomez M, et al. Microbiome-centered therapies for the management of metabolic dysfunction-associated steatotic liver disease. Clin Mol Hepatol 2025;31:S94-s111.
12. Rønne ME, Dybdahl Andersen C, Teze D, Petersen AB, Fredslund F, Stender EGP, et al. Action and cooperation in alginate degradation by three enzymes from the human gut bacterium Bacteroides eggerthii DSM 20697. J Biol Chem 2024;300:107596.
13. Tiemblo Martín M, Coccimiglio M, Andretta E, De Simone Carone L, Bell A, Gerpe-Amor T, et al. The human gut Bacteroides eggerthii expresses a new galactofuranose-containing lipooligosaccharide with weak immunostimulatory properties. Carbohydr Polym 2025;348:122833.
14. Gauffin Cano P, Santacruz A, Moya Á, Sanz Y. Bacteroides uniformis CECT 7771 ameliorates metabolic and immunological dysfunction in mice with high-fat-diet induced obesity. PLoS One 2012;7:e41079.
15. López-Almela I, Romaní-Pérez M, Bullich-Vilarrubias C, Benítez-Páez A, Gómez Del Pulgar EM, Francés R, et al. Bacteroides uniformis combined with fiber amplifies metabolic and immune benefits in obese mice. Gut Microbes 2021;13:1-20.
16. Tilg H, Adolph TE, Trauner M. Gut-liver axis: Pathophysiological concepts and clinical implications. Cell Metab 2022;34:1700-1718.
17. Loomba R, Seguritan V, Li W, Long T, Klitgord N, Bhatt A, et al. Gut microbiome-based metagenomic signature for non-invasive detection of advanced fibrosis in human nonalcoholic fatty liver disease. Cell Metab 2017;25:1054-1062.e1055.
18. Oh TG, Kim SM, Caussy C, Fu T, Guo J, Bassirian S, et al. A

Universal gut-microbiome-derived signature predicts cirrhosis. Cell Metab 2020;32:878-888.e876.
19. Alferink LJM, Radjabzadeh D, Erler NS, Vojinovic D, Medina-Gomez C, Uitterlinden AG, et al. Microbiomics, metabolomics, predicted metagenomics, and hepatic steatosis in a population-based study of 1,355 adults. Hepatology 2021;73:968-982.
20. Frost F, Kacprowski T, Rühlemann M, Pietzner M, Bang C, Franke A, et al. Long-term instability of the intestinal microbiome is associated with metabolic liver disease, low microbiota diversity, diabetes mellitus and impaired exocrine pancreatic function. Gut 2021;70:522-530.
21. Plovier H, Everard A, Druart C, Depommier C, Van Hul M, Geurts L, et al. A purified membrane protein from Akkermansia muciniphila or the pasteurized bacterium improves metabolism in obese and diabetic mice. Nat Med 2017;23:107-113.
22. Liu Y, Zhu J, Wang H, Lu W, Lee YK, Zhao J, et al. Machine learning framework for gut microbiome biomarkers discovery and modulation analysis in large-scale obese population. BMC Genomics 2022;23:850.
23. López-Contreras BE, Morán-Ramos S, Villarruel-Vázquez R, Macías-Kauffer L, Villamil-Ramírez H, León-Mimila P, et al. Composition of gut microbiota in obese and normal-weight Mexican school-age children and its association with metabolic traits. Pediatr Obes 2018;13:381-388.
24. Assmann TS, Cuevas-Sierra A, Riezu-Boj JI, Milagro FI, Martínez JA. Comprehensive analysis reveals novel interactions between circulating microRNAs and gut microbiota composition in human obesity. Int J Mol Sci 2020;21:9509.
25. Yao L, Seaton SC, Ndousse-Fetter S, Adhikari AA, DiBenedetto N, Mina AI, et al. A selective gut bacterial bile salt hydrolase alters host metabolism. Elife 2018;7:e37182.
26. Nieminen MT, Hernandez M, Novak-Frazer L, Kuula H, Ramage G, Bowyer P, et al. DL-2-hydroxyisocaproic acid attenuates inflammatory responses in a murine Candida albicans biofilm model. Clin Vaccine Immunol 2014;21:1240-1245.
27. Park B, Hwang H, Chang JY, Hong SW, Lee SH, Jung MY, et al. Identification of 2-hydroxyisocaproic acid production in lactic acid bacteria and evaluation of microbial dynamics during kimchi ripening. Sci Rep 2017;7:10904.